Synergistic action of nectins and cadherins generates the mosaic cellular pattern of the olfactory epithelium

Sayaka Katsunuma,[1,2] Hisao Honda,[3,4] Tomoyasu Shinoda,[7] Yukitaka Ishimoto,[8] Takaki Miyata,[7] Hiroshi Kiyonari,[5,6] Takaya Abe,[6] Ken-ichi Nibu,[2] Yoshimi Takai,[1,9,10] and Hideru Togashi[1]

[1]Division of Molecular and Cellular Biology, Department of Biochemistry and Molecular Biology, [2]Department of Otolaryngology-Head and Neck Surgery, and [3]Division of Neural Differentiation and Regeneration, Department of Physiology and Cell Biology, Kobe University Graduate School of Medicine, Kobe 650-0017, Japan
[4]Laboratory for Morphogenetic Signaling, RIKEN Center for Developmental Biology, Kobe 650-0047, Japan
[5]Animal Resource Development Unit and [6]Genetic Engineering Team, Division of Bio-function Dynamics Imaging, RIKEN Center for Life Science Technologies, Kobe 650-0047, Japan
[7]Department of Anatomy and Cell Biology, Nagoya University Graduate School of Medicine, Nagoya 466-8550, Japan
[8]Department of Machine Intelligence and Systems Engineering, Akita Prefectural University, Akita 015-0055, Japan
[9]Division of Pathogenetic Signaling, Department of Biochemistry and Molecular Biology, Kobe University Graduate School of Medicine, Kobe 650-0047, Japan
[10]CREST, Japan Science and Technology Agency, Kobe 650-0047, Japan

In the olfactory epithelium (OE), olfactory cells (OCs) and supporting cells (SCs), which express different cadherins, are arranged in a characteristic mosaic pattern in which OCs are enclosed by SCs. However, the mechanism underlying this cellular patterning is unclear. Here, we show that the cellular pattern of the OE is established by cellular rearrangements during development. In the OE, OCs express nectin-2 and N-cadherin, and SCs express nectin-2, nectin-3, E-cadherin, and N-cadherin. Heterophilic trans-interaction between nectin-2 on OCs and nectin-3 on SCs preferentially recruits cadherin via α-catenin to heterotypic junctions, and the differential distributions of cadherins between junctions promote cellular intercalations, resulting in the formation of the mosaic pattern. These observations are confirmed by model cell systems, and various cellular patterns are generated by the combinatorial expression of nectins and cadherins. Collectively, the synergistic action of nectins and cadherins generates mosaic pattern, which cannot be achieved by a single mechanism.

Introduction

The olfactory epithelium (OE), which is located inside the nasal cavity in mammals, is a specialized sensory epithelium that is involved in odor perception. The OE is a pseudostratified, columnar epithelium, and it comprises three predominant cell types: olfactory cells (OCs), supporting cells (SCs), and basal cells (Fig. S1 A). These cells are layered from the apical to the basal surface, respectively, in the OE. When the luminal surface of the OE is observed from the apical side, ciliated OCs and several types of SCs are arranged in a unique mosaic pattern (Fig. S1 A; Cuschieri and Bannister, 1975; Steinke et al., 2008). The most characteristic aspect of this cellular pattern is that the dendrites of OCs are enclosed by columnar, polygonal SCs. However, the mechanism responsible for this cellular patterning in the OE remains unclear.

In the OE, E-cadherin localizes at homotypic boundary between SCs (S-S boundary), whereas N-cadherin localizes at the S-S boundary and heterotypic boundary between OCs and SCs (O-S boundary; Steinke et al., 2008). These observations suggest that SCs express both E- and N-cadherin, whereas OCs express only N-cadherin. In mixed cultures of cell lines that express E- or N-cadherin, these cells form separate aggregates (Nose et al., 1988; Katsamba et al., 2009). However, in the OE, OCs and SCs intermingle with each other and form mosaic patterns.

We have reported that nectins regulate the checkerboard-like mosaic cellular patterning in the mouse auditory epithelium (Togashi et al., 2011). Nectins comprise a family of immunoglobulin-like molecules, consisting of four members: nectin-1, -2, -3, and -4. Nectins first form a cell–cell contact site and then recruit cadherins to this site to establish adherens junctions (AJs; Takai and Nakanishi, 2003). Thus, nectins are implicated in the formation of cadherin-based AJs. Nectins can engage in homophilic and heterophilic trans-interactions (Takahashi et al., 1999; Satoh-Horikawa et al., 2000). Their heterophilic trans-interactions are stronger than their homophilic trans-interactions in the following order: nectin-1–3 > nectin-2–3 > nectin-1–1, -2–2, and -3–3 (Fabre et al., 2002; Yasumi et al., 2003; Martinez-Rico et al., 2005; Harrison et al., 2012). This property of nectins contributes to the forma-

Correspondence to Hideru Togashi: htogashi@med.kobe-u.ac.jp

Abbreviations used in this paper: AJ, adherens junction; E, embryonic day; KO, knockout; OC, olfactory cell; OE, olfactory epithelium; P, postnatal day; SC, supporting cell; WT, wild type; ZO, zona occludens.

© 2016 Katsunuma et al. This article is distributed under the terms of an Attribution–Noncommercial–Share Alike–No Mirror Sites license for the first six months after the publication date (see http://www.rupress.org/terms). After six months it is available under a Creative Commons License (Attribution–Noncommercial–Share Alike 3.0 Unported license, as described at http://creativecommons.org/licenses/by-nc-sa/3.0/).

The Rockefeller University Press $30.00
J. Cell Biol. Vol. 212 No. 5 561–575
www.jcb.org/cgi/doi/10.1083/jcb.201509020

THE JOURNAL OF CELL BIOLOGY

Downloaded from http://rupress.org/jcb/article-pdf/212/5/561/1601018/jcb_201509020.pdf by guest on 08 February 2026

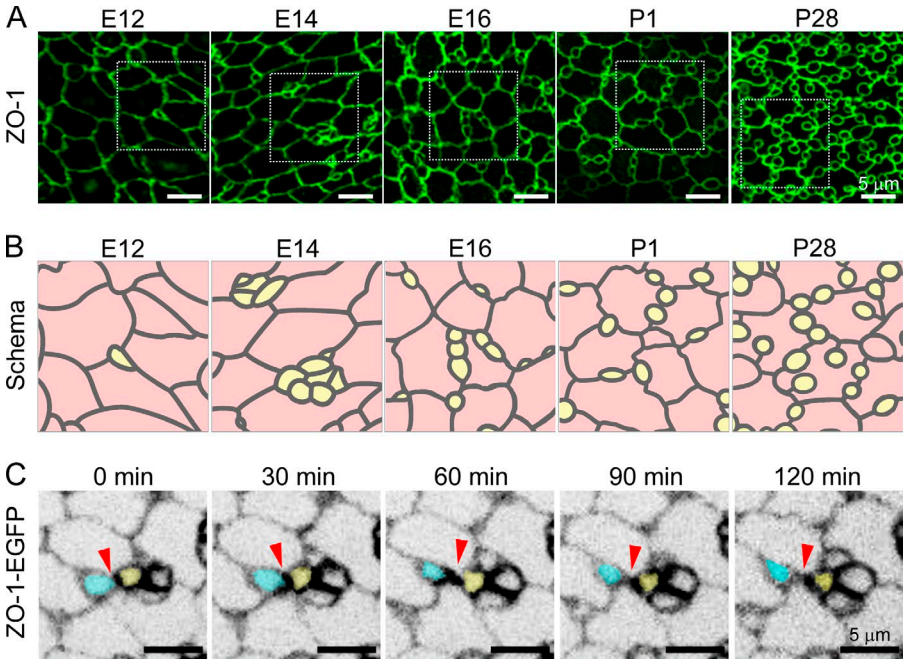

Figure 1. **Cellular rearrangements in the developing mouse OE.** (A) Immunostainings for ZO-1 on the apical surface of the mouse OE from E12 to P28. (B) Schematic presentation of each field inside the dashed-line square in each panel of A. Yellow, OCs; pink, SCs. (C) Time-lapse imaging of the organ culture of the OE derived from R26-ZO1-EGFP mice. Black and white reversal images at 30-min intervals are shown. Arrowheads indicate the separation of adjacent OCs (blue and yellow).

tion of heterophilic cell adhesion between multiple cell types (Ozaki-Kuroda et al., 2002; Inagaki et al., 2005; Togashi et al., 2011). In the mouse cochlea, nectin-1 and nectin-3 are differentially expressed in hair cells and supporting cells and their trans-interactions mediate the heterophilic adhesion between these two cell types, which contributes to the formation of a checkerboard-like pattern (Togashi et al., 2011).

The cadherin and nectin systems are physically and functionally associated during cell–cell junction formation through their intercellular interactions (Tachibana et al., 2000; Takai et al., 2008). Cooperative mechanisms between these adhesive systems likely contribute to the production of complex cell-sorting patterns, which cannot be achieved by a single mechanism (Takeichi, 2011). However, our current understanding of the cooperative roles between cadherins and nectins is not sufficient to entirely explain the complex mechanism underlying cellular patterning. In the present study, we examined the cooperative mechanism between cadherins and nectins in highly ordered cellular patterning using mouse OE as a model system.

Results

Cellular rearrangements during the formation of the mosaic cellular pattern of the OE

To examine how the mosaic cellular pattern is organized, we first investigated cellular patterning in the OE at different developmental stages by immunostaining for zona occludens-1 (ZO-1), a representative marker for cell junctions (Fig. 1 A). The mouse OE develops between embryonic day 9 (E9) and E10. Dendrites of OCs first appear on the surface of the OE around E11. On E12, a few OCs could be detected in the OE. Dendrites of immature OCs were distinguished by immunostaining for MAP2 (Fig. S1 B). On E14, the number of OC dendrites that appeared on the surface of the OE increased, and several dendrites formed clusters at the S-S boundary. By E16, OCs contacted each other and gradually aligned at the S-S boundary. OCs gradually separated from each other and became interspersed with, and surrounded by, SCs. OCs were located at the S-S boundary between neighboring SCs from E18 to postnatal day 1 (P1). On P28, some OCs were sheathed within a single SC, and the characteristic cellular pattern was established. These observations, which are schematically shown in Fig. 1 B, suggested that the maturation of the OE was accompanied by cellular rearrangements during development. Quantitative analysis revealed that approximately one half of the OCs appeared in isolation at the time of their appearance on the surface of the OE (Fig. S1 C).

To investigate cell behavior in living tissue, we generated a transgenic mouse line (R26-ZO1-EGFP) that ubiquitously expresses EGFP fused to mouse ZO-1 under the control of the *ROSA26* locus (Abe et al., 2011). This allowed continuous, fluorescent labeling of all boundaries. Live imaging of the apical surface of an organ culture of the OE prepared on E14 revealed that OCs, which initially adhered to each other in the cluster, gradually separated (Fig. 1 C and Video 1). These observations directly indicated that cellular rearrangements played a role in the mosaic cellular patterning of the OE.

Differential distribution and expression patterns of nectins in the developing OE

We then examined the distribution patterns of nectin-1, -2, and -3 in the OE on P28 (Fig. 2 A). At this stage, nectin-1 was hardly detected in the OE. Nectin-2 was uniformly distributed at the O-S and S-S boundaries, and nectin-3 prominently localized at the S-S boundary and faintly localized at the O-S boundary. In a lateral view of the OE, all of the nectins were concentrated at the apical area where AJs were located (Fig. 2 B).

To identify the cells expressing nectin-1, -2, and -3, we performed in situ hybridizations on P28 (Fig. 2 C). The nuclei of SCs form a superficial layer, and OCs are distinguished by OMP (olfactory marker protein) staining. Nectin-2 mRNA was detected in OCs and SCs, whereas nectin-3 mRNA was detected in SCs. Nectin-1 was detected in OCs and SCs; however, the signal for nectin-1 mRNA was weak.

Downloaded from http://rupress.org/jcb/article-pdf/212/5/561/1601018/jcb_201509020.pdf by guest on 08 February 2026

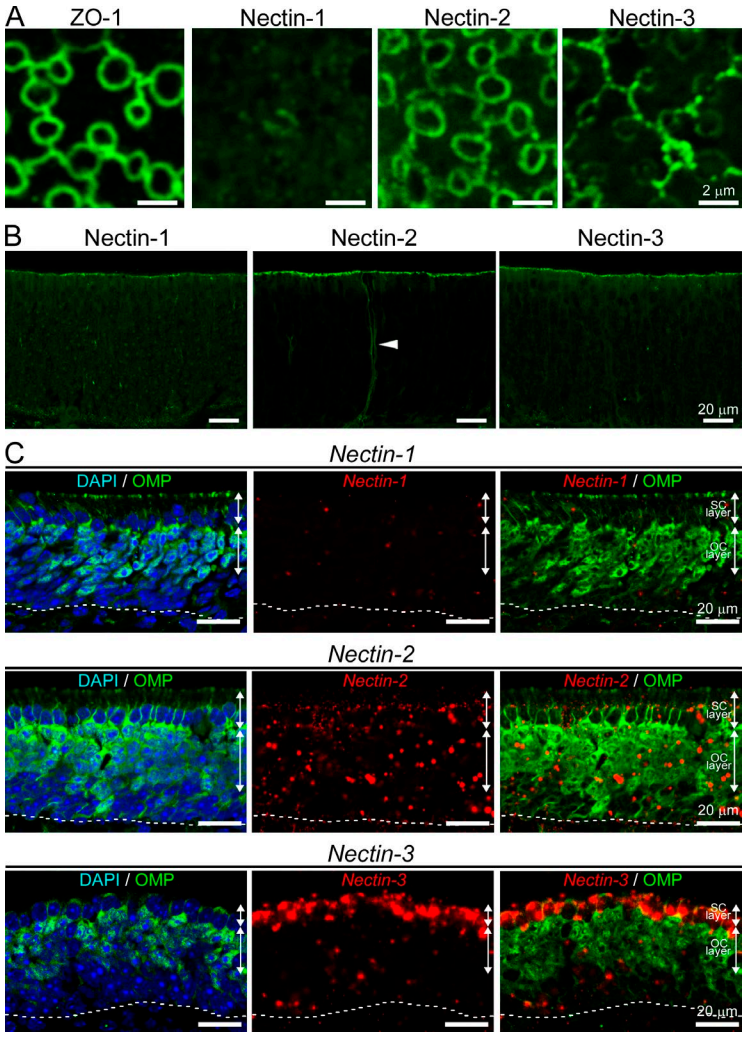

Figure 2. **Distribution and expression patterns of nectins in the mouse OE.** (A) Immunostainings for ZO-1, nectin-1, -2, and -3 in the OE on P28. (B) Immunostainings for nectins in sections of the mouse OE on P28. Arrowhead indicates Bowman's gland. The reason why the reactivity of the anti-nectin-1 antibody tends to increase in the OE sections is unknown. (C) In situ hybridizations in sections of the OE on P28. Each panel shows staining for DAPI (blue), OMP (green), and mRNA for each nectin (red). Dotted lines show the basal lamina. The two-way arrows indicate SC or OC layers.

Next, we examined changes in the distributions of nectin-2 and -3 during cellular rearrangements in the OE from E14 to P1 (Fig. 3 A). On E14, nectin-2 was primarily detected at the boundary between clustered, neighboring OCs (O-O boundary) and weakly detected at the S-S and O-S boundary. On E16, nectin-2 was prominently detected at the O-S and O-O boundary, whereas it was weakly detected at the S-S boundary. From E18 to P1, nectin-2 was prominently distributed at the O-S boundary and weakly distributed at the S-S boundary. We then examined the distribution pattern of nectin-3 on E14. Nectin-3 was prominently detected at the S-S boundary, whereas it was weakly detected at the O-S boundary. On E16, nectin-3 was prominently detected at the O-S boundary and S-S boundary. On E18, nectin-3 was distributed at the O-S and S-S boundary. On P1, nectin-3 was prominently distributed at the S-S boundary, whereas it was weakly detected at the O-S boundary. These observations suggested that nectin-2 on OCs preferentially recruited nectin-3 that was present on the SC membranes. Thus, the heterophilic trans-interaction between nectin-2 on OCs and nectin-3 on SCs might be involved in mosaic cellular patterning. In the mature OE, nectin-3 was prominently distributed at the S-S boundary, and it was weakly distributed at the O-S boundary; the mechanistic details of these distributions are described later (Fig. S4). A summary of the distribution patterns of nectins during development is shown in Fig. S2.

To verify the hypothesis that the heterophilic trans-interaction between nectin-2 and -3 regulates cellular rearrangements, we analyzed the cellular patterns of the OE of mice in which nectin-1, -2, or -3 gene was knocked out (Fig. 3 B). There were no differences in the number of OCs in these nectin knockout (KO) mice (Fig. 3 C). However, the cellular patterns were altered in nectin-2 KO and nectin-3 KO mice. On P28, OCs in these KO mice did not separate from each other, and two or three OCs were attached to each other (Fig. 3 B, arrowheads). Attached OCs were more frequently observed in nectin-3 KO mice than in nectin-2 KO mice. We also analyzed the cellular patterns of the OE of mice in which nectin -2 and -3 genes were both knocked out (N2/N3 KO; Fig. 3 B). Attached OCs observed in N2/N3 KOs were similar to those observed in nectin-3 KOs (Fig. 3 C). In contrast, nectin-1 KO mice did not show any abnormal phenotypes. These results indicated that nectin-2 or -3 deficiency prevented the separation of attached OCs, suggesting that the heterophilic trans-interaction between nectin-2 and -3 was involved in cellular rearrangements of the developing OE.

Differential distribution and expression patterns of cadherins and catenins in the developing OE

As nectins are known to cooperate with the cadherin–catenin complex in the formation of AJs (Tachibana et al., 2000), we

Downloaded from http://rupress.org/jcb/article-pdf/212/5/561/1601018/jcb_201509020.pdf by guest on 08 February 2026

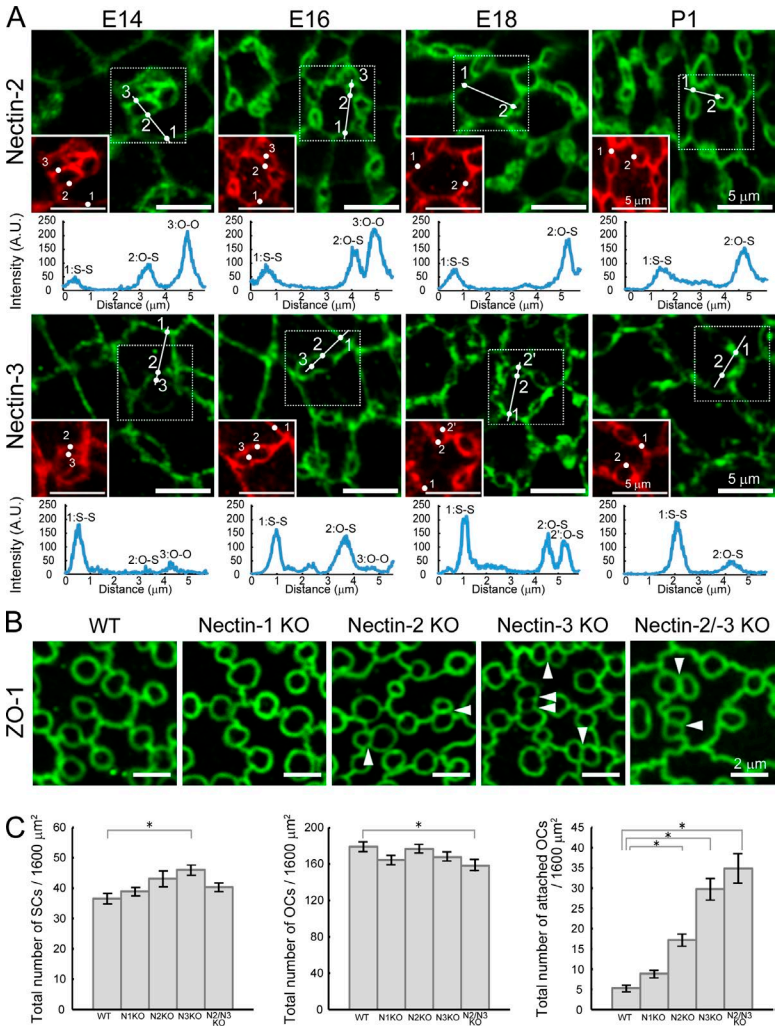

Figure 3. **Distribution change of nectins in the developing mouse OE and the phenotypes of nectin KO mice.** (A) Distribution patterns of nectin-2 (top) and -3 (bottom) in the OE during development. Immunostaining for nectin-2 or -3 (green) is shown. Insets show immunostaining for afadin (red), which indicates all boundaries. A representative image is shown of six independent experiments. The graphs indicate the densitometric traces of the lines in the photographs of nectin fluorescence. Peaks correspond to the signals at the junction marked with the same number in the upper figures. S-S, junction between SCs; O-S, junction between OCs and SCs; O-O, junction between OCs. (B) The cellular patterns of the OE derived from WT or nectin KO mice on P28. Immunostaining for ZO-1 is shown. Arrowheads indicate attached OCs. (C) Statistical analysis of nectin-KO phenotypes on P28. Left, number of SCs; middle, number of OCs; right, number of attached OCs. Results shown are the mean ± SD; *, $P < 0.001$. $n = 9$.

examined the distribution patterns of cadherins and the cadherin-associated proteins, catenins, in the OE (Fig. 4 A). On P28, E-cadherin was prominently concentrated at the S-S boundary, whereas it was faintly distributed at the O-S boundary. N-cadherin was concentrated mainly at the O-S boundary, whereas it was weakly concentrated at the S-S boundary on P28. In a lateral view of the OE, all of the cadherin and catenin molecules were concentrated at the apical area where AJs were located, and they were more broadly distributed toward the basal side of AJs (Fig. 4 B). To identify cells expressing E- and N-cadherin, we performed in situ hybridizations with staining for OMP on P28. E-cadherin mRNA was detected only in SCs, whereas N-cadherin mRNA was detected in OCs and SCs (Fig. 4 C).

We then examined the distribution patterns of β-catenin, αE-catenin, and αN-catenin on P28 (Fig. 4 A). β-Catenin, a representative marker of the cadherin–catenin complex that binds to the classic cadherin members, was distributed mainly at the S-S boundary and weakly at the O-S boundary. αE-catenin was concentrated at the S-S boundary, whereas it was faintly concentrated at the O-S boundary. αE-catenin showed essentially the same distribution pattern as seen for E-cadherin. αN-Catenin was detected at the circumferential rings around OCs, but not at the S-S boundary. These observations implied that αE-catenin was expressed in SCs and that αN-catenin was expressed in OCs. It is noted that these distribution patterns of cadherins and β-catenins in the adult mouse are consistent with earlier observations (Steinke et al., 2008).

We next examined developmental changes in the distribution patterns of β-catenin as a marker for the cadherin–catenin complex during cellular rearrangements in the OE from E14 to P1 (Fig. 5 A). On E14, β-catenin was prominently concentrated at the S-S boundary, but it was weakly detected at O-S and O-O boundary (Figs. 5 A and S2). From E14 to E16, β-catenin was continuously prominent at the S-S boundary; however, β-catenin at the O-S boundary became more prominent on E16. From E18 to P1, β-catenin was prominently detected at the S-S boundary; however, β-catenin gradually decreased at the O-S boundary, which was followed by the separation of attached OCs.

E-cadherin and αE-catenin were always prominently localized at the S-S boundary, whereas they were barely detected at the O-S boundary. N-cadherin was uniformly distributed at the junctions in the OE on E14. However, from E16 to P1, N-cadherin at the S-S boundary decreased and, consequently, N-cadherin at the O-S boundary became more prominent compared with that at the S-S boundary (Fig. S3). αN-Catenin was uniformly concentrated at the O-S and O-O boundary from E14 to P1. Distribution patterns of cadherins and catenins during development are shown in Fig. S3 and summarized in Fig. S2.

Downloaded from http://rupress.org/jcb/article-pdf/212/5/561/1601018/jcb_201509020.pdf by guest on 08 February 2026

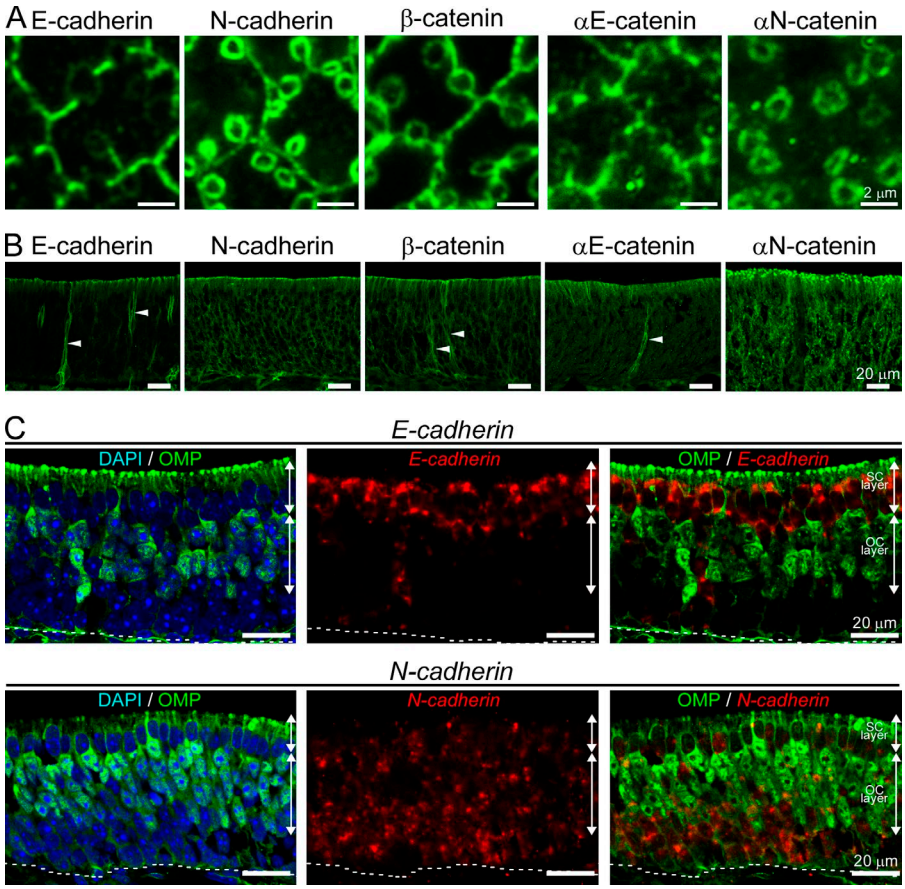

Figure 4. **Distribution and expression patterns of cadherins and catenins in the mouse OE.** (A) Immunostainings for E-cadherin, N-cadherin, β-catenin, αE-catenin, and αN-catenin in the OE on P28. (B) Immunostainings for E-cadherin, N-cadherin, β-catenin, αE-catenin, and αN-catenin in sections of the mouse OE on P28. Arrowheads indicate Bowman's glands. (C) In situ hybridizations in sections of the OE on P28. Each panel shows the staining for DAPI (blue), OMP (green), and mRNA for each cadherin (red). Dotted lines show the basal lamina. The two-way arrows indicate SC or OC layers.

Requirement of αN-catenin for the cooperation between nectins and cadherins in mosaic cellular patterning of the OE

We then assessed the effect of cadherin inactivation on cellular patterning of the OE using αN-catenin KO mice (Togashi et al., 2002). When α-catenin is inactivated, cadherin function is perturbed (Hirano et al., 1992; Watabe et al., 1994); however, homophilic trans-interactions of cadherins via the extracellular domain still occur. α-Catenin is also implicated in the cooperation between nectins and cadherins (Tachibana et al., 2000). We examined cellular patterning in αN-catenin KO mice on P0, because αN-catenin KO mice die within 24 h after birth (Togashi et al., 2002). The numbers of OCs and SCs were not altered in αN-catenin KO mice on P0 (Fig. 5 C). However, in αN-catenin KO mice, OCs aberrantly attached to each other, as revealed by immunostaining for ZO-1, and the cellular pattern was severely affected (Fig. 5 B, arrowheads). Although the absolute number of attached olfactory cells was only double in the αN-catenin KO mouse, the percentage was near the percentage found at E14 and E16 in wild-type (WT) mice. Thus, the OE development was essentially halted in αN-catenin KO mice.

To understand how the aforementioned phenotypes were generated, we examined changes in the distribution of β-catenin in the OE of αN-catenin KO mice from E14 to E16 (Fig. 5, D and E). The numbers of OCs and SCs and the cellular patterns in αN-catenin KO mice on E14 were not different from those in WT mice. These observations indicated that the cellular pattern defect of αN-catenin KO mice was not caused by a developmental delay. On E14, β-catenin accumulated at the S-S boundary, whereas it was not particularly concentrated at the O-S or O-O boundary, and the distribution patterns of β-catenin did not differ between WT and αN-catenin KO mice. On E16, β-catenin accumulation at the S-S boundary did not differ between WT and αN-catenin KO mice. At the O-S boundary of WT mice, β-catenin became more prominent; however, in those of αN-catenin KO mice, β-catenin accumulation did not increase. Thus, the relative distributions of the cadherin–catenin complex between the O-S and S-S boundary were altered in αN-catenin KO mice on E16. These observations suggest that αN-catenin is required for β-catenin accumulation at the O-S boundary in the OE.

Mathematical modeling of mosaic cellular patterning

Differential adhesion has been proposed to promote cell rearrangements and cell sorting in cell aggregates (Foty and Steinberg, 2005; Steinberg, 2007). Cell sorting and cell rearrangements are driven by a diminution of adhesive free energy as cells tend to maximize their mutual binding, which drives strongly adhesive cells together and weakly adhesive cells out. Differential adhesions could drive self-organized cell movements of the OE. We hypothesized that the heterophilic trans-interaction between nectin-2 on OCs and nectin-3 on SCs might preferentially promote the recruitment of the cadherin–catenin complex to the heterotypic boundary, and the differential distributions of the cadherin–catenin complex might provide the differential adhesion required for their cellular rearrangements (Fig. 6 A).

To test this idea, we mathematically modeled the vertex dynamics of polygonal cells (Honda et al., 2004, 2008). The model can be used for a polygonal pattern in which polygons are packed in a 2D sheet and consist of many polygon edges.

Downloaded from http://rupress.org/jcb/article-pdf/212/5/561/1601018/jcb_201509020.pdf by guest on 08 February 2026

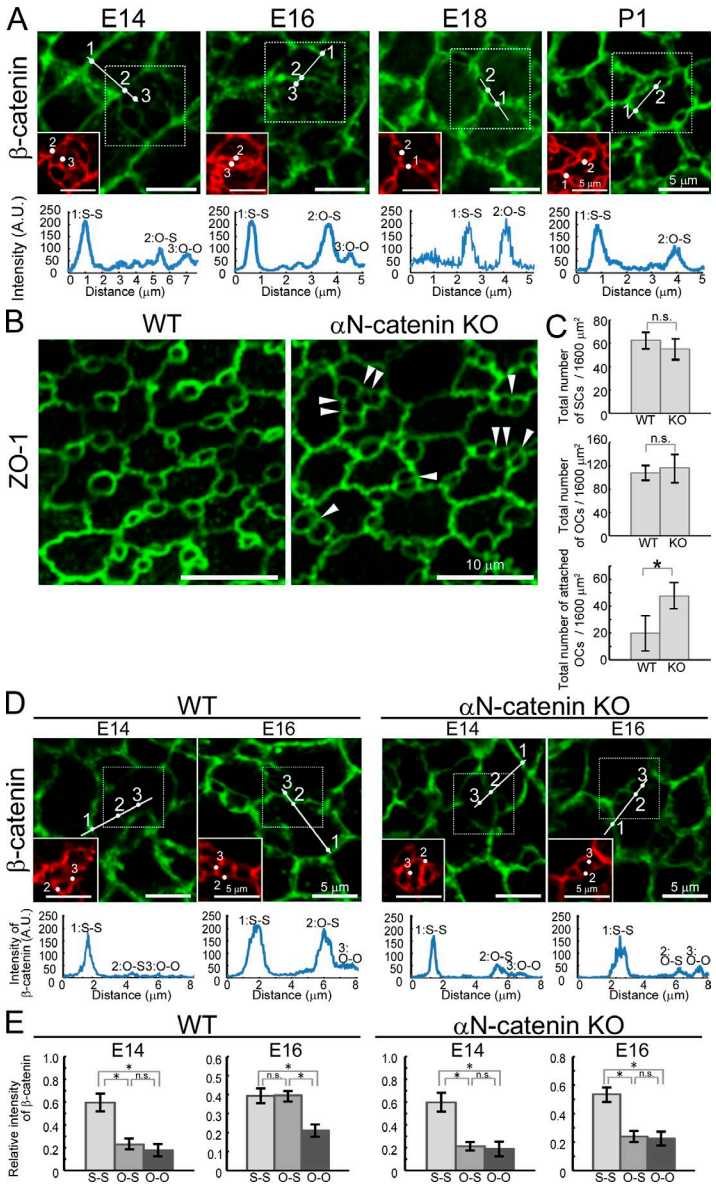

Figure 5. **Distribution change of cadherin-catenin complex in the developing mouse OE and the phenotypes of αN-catenin KO mice.** (A) Immunostaining for β-catenin in the developing mouse OE. Insets show immunostaining for ZO-1 (red), which indicates all boundaries. A representative image is shown of six independent experiments. The graph notations are the same as those in Fig. 3 A. (B) The cellular patterns in the OE derived from WT or αN-catenin KO mice on P0. The immunostaining for ZO-1 is shown. Arrowheads indicate attached OCs. (C) Statistical analysis of αN-catenin-KO phenotypes on P0. Top: number of SCs. Middle: number of OCs. Bottom: number of aberrant attached OCs. Results shown are the mean ± SD; *, $P < 0.001$. $n = 9$. (D) Immunostaining for β-catenin in the OE of WT (left) or αN-catenin KO (right) mice on E14 and E16. Insets show immunostaining for ZO-1 (red). A representative image is shown of six independent experiments. The graph notations are the same as those in Fig. 3 A. (E) Statistical analysis for the normalized fluorescence intensity of β-catenin in the OE of WT (left) or αN-catenin KO (right) mice on E14 and E16. Results shown are the mean ± SD; *, $P < 0.001$. $n = 9$.

Two different types of polygons were placed on the sheet (i.e., yellow polygons [O] and pink polygons [S]; Fig. 6 B). We simulated two cases of cellular pattern: one when the adhesiveness of polygon edges S-S, O-S, and O-O were 1.0, 1.0, and 0.588, respectively (Fig. 6 B, left), and the other with the weaker differential adhesiveness 0.833 of the O-S edges (Fig. 6 B, right). A common initial configuration was constructed with the adhesiveness 1.0, 0.833, and 0.588 for S-S, O-S, and O-O, respectively, where two O polygons initially adhered to one another via a vertical edge. In the former, this O-O edge shortened at step 1,500 and was then replaced with a new, horizontal S-S edge at step 2,300. In the following steps, the adhesiveness of the O-S edges was reduced from 1.0 to 0.89, which corresponded with the observation that β-catenin intensity decreased on P1 (Fig. 5 A). The horizontal S-S edge was elongated strongly at step 4,000. In contrast, in the latter case, the O-O edge kept its initial arrangement when the adhesiveness of the O-S kept 0.833. These results were similar to those observed in the OE (Fig. 1 C) and supported the idea that the differential adhesiveness between OCs and SCs drove cell intercalations.

Requirements of nectin and cadherin activities for mosaic cellular patterning

We then examined the relationship between differential expression patterns of cadherins and cellular patterning. It is known that cells expressing different types of cadherins are segregated from each other (Nose et al., 1988; Takeichi, 1990; Katsamba et al., 2009). When cells expressing either E- or N-cadherin were randomly mixed and cultured for 72 h, these cells segregated from each other (Video 2). As mentioned in the previous section, OCs expressed N-cadherin and SCs expressed E- and N-cadherin. We prepared HEK293 (293) cells stably expressing N-cadherin and/or E-cadherin to clarify whether differential expression of cadherins is implicated in cellular patterning; 293 cells naturally express N-cadherin, but not E-cadherin (Hogan et al., 2004). We performed a mosaic-forming assay to examine the differences in cellular patterning between the 293 transfectants (Fig. 7 A). In the mosaic-forming assay, two different transfectants, which expressed EGFP or mCherry to distinguish them, were seeded into two wells that were separated by an insert. Then, the culture insert was removed to form an artificial boundary between the cells. When their

Downloaded from http://rupress.org/jcb/article-pdf/212/5/561/1601018/jcb_201509020.pdf by guest on 08 February 2026

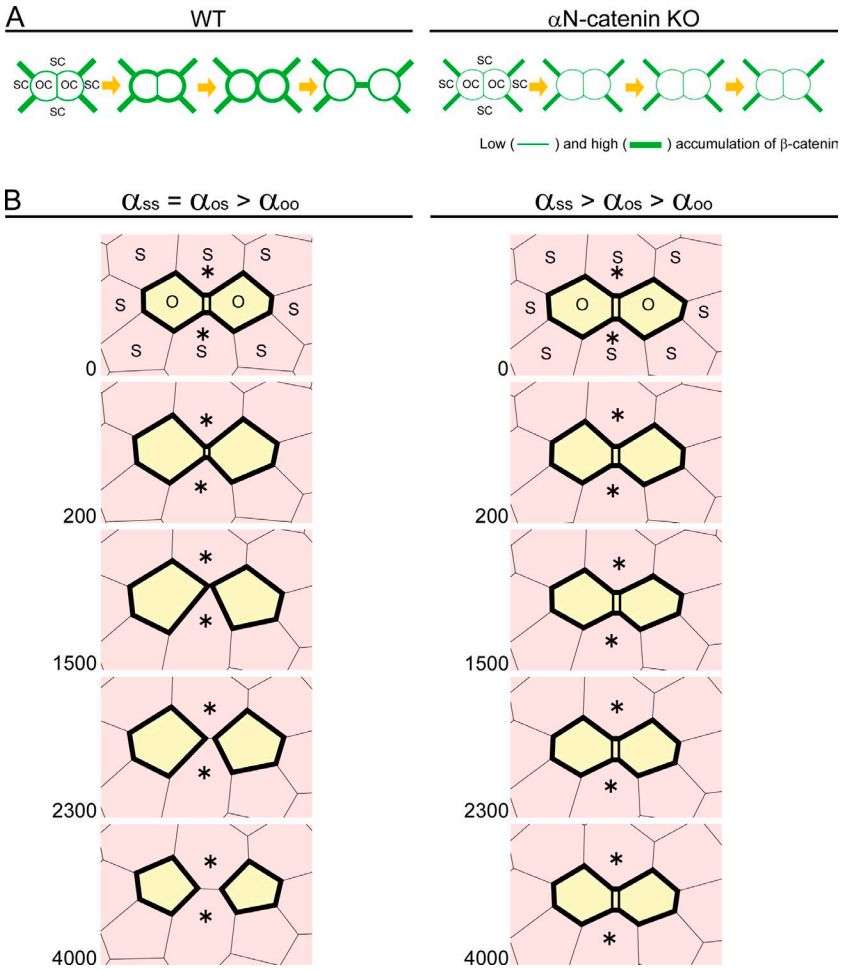

Figure 6. **Mathematical modeling of cell junctional rearrangements.** (A) Schematic illustrations of cellular rearrangements and changes in the distribution of β-catenin in WT (left) or αN-catenin KO (right) mice during development. (B) Mathematical modeling of cell junctional rearrangements. (left) Polygonal cellular patterns are shown for the case in which heterophilic interactions between O polygons (O) and S polygons (S) are as strong as homophilic interactions between S polygons (S-S = O-S > O-O, adhesiveness strengths α_{ss} = α_{os} = 1.0, α_{oo} = 0.533. Steps 0–2,300). The O-O edge was then replaced with a new contact formed between S polygons (asterisks). The horizontal edges were elongated after step 2,300 (α_{os} = 0.89). (right) Intercalation did not occur between O and S polygons when heterophilic interactions between O and S polygons are weaker than homophilic interactions between S polygons (i.e., S-S > O-S > O-O, α_{ss} = 1.0, α_{os} = 0.833, α_{oo} = 0.533). Bold lines, O-S boundary; narrow lines, S-S boundary; double lines, O-O boundary. See Materials and methods for details.

colony borders came into contact with one another, their boundaries were examined; 293 transfectants expressing both E- and N-cadherin and those expressing N-cadherin did not intermingle at the border, nor did cells expressing the same cadherin. These results indicated that the homophilic trans-interactions between cadherins alone could not explain the mosaic cellular patterning.

We then examined the roles of the heterophilic trans-interaction between nectin-2 and -3 in cellular patterning. We prepared 293 cells stably expressing nectin-2 (n2-293) or -3 (n3-293), as well as EGFP or mCherry, respectively, to distinguish between them. We performed the mosaic-forming assay to examine the cellular patterning of these cells (Fig. 7 B). In control experiments, the cells expressing identical nectin types were not intermingled, whereas n2- and n3-293 cells intermingled with each other. In this assay, cellular intermingling between the colonies could be the result of continuous intercalation of the cells. Nectin-1, -2, and -3 have a conserved PDZ binding motif at their cytoplasmic C terminus that binds afadin (Takai et al., 2008), and the interactions between nectins and afadin are required for the efficient recruitment of the cadherin–catenin complex via α-catenin to the nectin-based cell–cell adhesion sites (Tachibana et al., 2000; Sato et al., 2006). We determined whether the PDZ binding motif of nectins is required for mosaic cellular patterning by using truncated PDZ binding motif constructs of nectin-2 (n2Δ) or nectin-3 (n3Δ). The cells stably expressing these truncated constructs failed to intermingle at the border in the mosaic-forming assay (Fig. 7 B). These results suggested that the PDZ binding motif of nectins was necessary for mosaic cellular patterning.

We have reported that nectin-1 and -3 are more intensely localized at the heterophilic interfaces between n1- and n3-293 cells compared with the homotypic interfaces of n1- or n3-293 cells, and β-catenin is always highly concentrated at sites of nectin condensation between n1- and n3-293 cells (Togashi et al., 2006). To examine how the heterophilic trans-interaction (nectin-2–nectin-3 [n2–n3]) and the homophilic trans-interaction (nectin-2–nectin-2 [n2–n2] or nectin-3–nectin-3 [n3–n3]) affect the localization of nectins at cell interfaces, we examined cell boundaries in a mixed culture of n2- and n3-293 cells (Fig. 7 C). Nectin-3 was more intensely localized at the heterotypic n2–n3 cell boundary than at the homotypic n3–n3 cell boundary. In contrast, nectin-2 uniformly localized at both the homotypic and heterotypic boundaries. Consequently, the junctional accumulation of β-catenin increased at heterotypic n2–n3 cell boundary, whereas it decreased at homotypic n2–n2 or n3–n3 cell boundary. We then examined how the heterophilic trans-interactions between nectin-2Δ and -3Δ affect the recruitment of β-catenin at cell interfaces in a mixed culture of n2Δ- and n3Δ-293 cells (Fig. 7 C). Nectin-2Δ was diffusely distributed throughout the membrane, and nectin-3Δ was faintly detected at cell–cell boundaries. In these cultures, β-catenin was also faintly detected at cell–cell boundaries, and there was no difference in the accumulation of β-catenin between the heterotypic and homotypic boundaries. These observations indicated that the truncated PDZ binding motif mutants of nectins failed to efficiently recruit β-catenin at cell–cell boundaries. These results suggested that the differential distributions of the

Downloaded from http://rupress.org/jcb/article-pdf/212/5/561/1601018/jcb_201509020.pdf by guest on 08 February 2026

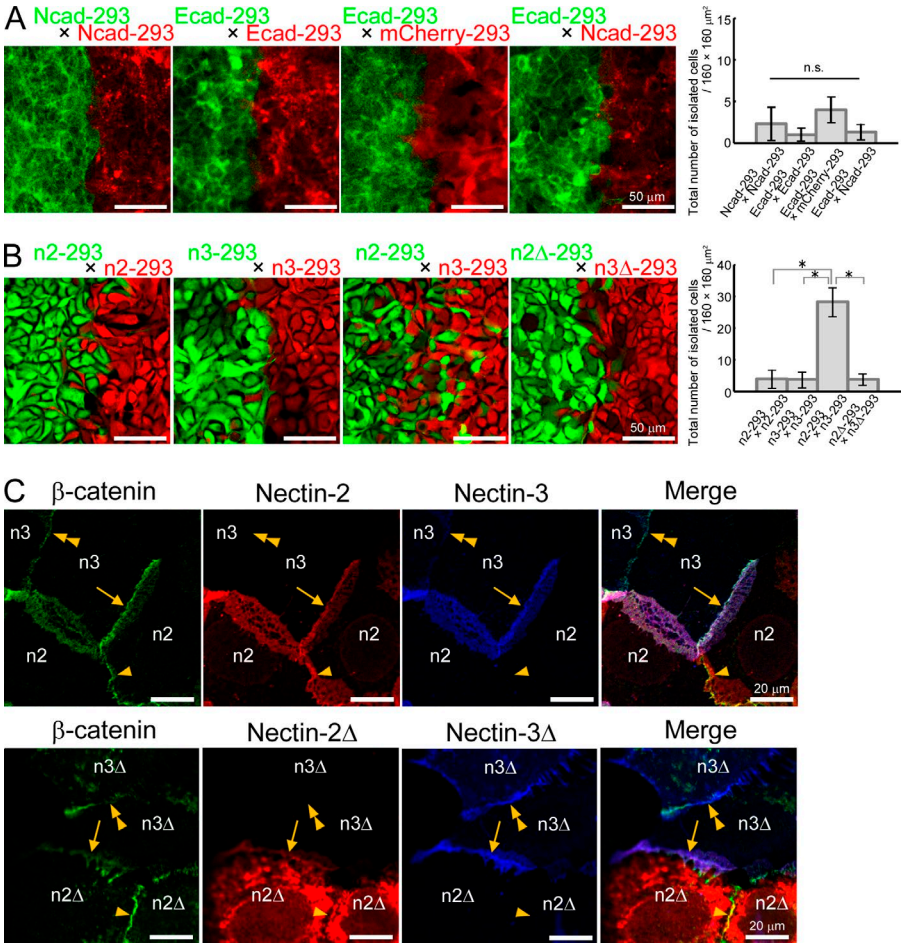

Figure 7. **Requirements of nectin and cadherin activities for mosaic cellular patterning.** (A) Mosaic-forming assay using HEK293 (293) cells expressing different combinations of cadherins. Boundaries between two colonies of cells, which were transfected with E-cadherin-EGFP (Ecad-293, green), E-cadherin-mCherry (Ecad-293, red), N-cadherin-EGFP (Ncad-293, green), N-cadherin-mCherry (Ncad-293, red), or mCherry (mCherry-293, red) in the indicated combinations. The graph shows the number of singly isolated cells in the mixtures of the two cell populations in each field. The results shown are the mean ± SD; n.s., not significant. $n = 6$. (B) Mosaic-forming assay using 293 cells expressing different combinations of nectins. Boundaries between two colonies of 293 transfectants are shown. The cells were doubly transfected with a nectin or truncated nectin (nectinΔ) and EGFP or mCherry. n2-293, 293 nectin-2 transfectants; n3-293, nectin-3 transfectants; n2Δ-293, nectin-2Δ transfectants; n3Δ-293, nectin-3Δ transfectants. The graph shows the number of singly isolated cells in the mixtures of the two cell populations in each field. The results shown are the mean ± SD; *, $P < 0.001$. $n = 6$. (C) Distributions of nectins and β-catenin in a mixed culture of nectin transfectants; 293 transfectants were mixed and triple stained for β-catenin (green), nectin-2 or nectin-2Δ (red), and nectin-3 or nectin-3Δ (blue). The panels show immunostaining in the mixed culture of n2- and n3-293 cells (top) or n2Δ- and n3Δ-293 cells (bottom). Arrows, heterotypic junctions; arrowheads, homotypic junctions between n2–n2 or n2Δ–n2Δ; double arrowheads, homotypic junctions between n3–n3 or n3Δ–n3Δ.

cadherin–catenin complex at the heterotypic boundary might be the driving force for intercalations between the homotypic boundary in the mosaic-forming assay.

Next, we determined whether cadherin activity is required for nectin-dependent mosaic cellular patterning using neuro-2a (n2a) cells (Fig. 8 A). N2a cells, a mouse neuroblastoma cell line, are cadherin deficient. We prepared n2a transfectants expressing nectin-2 (n2–n2a) or -3 (n3–n2a), as well as EGFP or mCherry, respectively. All n2a nectin transfectants failed to form tight and stable intercellular contacts, and the cells moved randomly between gaps in the cells as if they were not affected by each other (Fig. 8 A). Thus, n2a nectin transfectants did not show any differences in the mosaic-forming assay. We then prepared n2a transfectants that expressed both nectins and cadherins to examine the role of cadherins in cellular patterning (Fig. 8 A). In the mosaic-forming assay, these transfectants firmly attached to each other, and cells expressing nectin-2 and E-cadherin ([n2+Ecad]–n2a) and those expressing nectin-3 and E-cadherin ([n3+Ecad]–n2a) intermingled with each other. In contrast, cells expressing identical nectins and cadherins did not intermingle with each other. These observations indicated that cadherin activity was required for nectin-dependent mosaic cellular patterning.

We wondered why nectin-3 in the OE localized mainly to the S-S boundary and was hardly detected at O-S boundary from P1 onward. We suspected that the simultaneous expression of nectin-2 and -3 in SCs might be responsible for this distribution. To test this idea, we prepared 293 cells stably expressing both nectin-2 and -3 ([n2+n3]-293) and examined the localizations of nectins in confluent cultures (Fig. S4). In the cultures, three types of interfaces were formed: n2–n2, [n2+n3]–[n2+n3], and n2–[n2+n3]. Nectin-2 was uniformly localized at all the cell interfaces; however, nectin-3 prominently localized at the interface of confluent [n2+n3]–[n2+n3] cells. These results indicated that nectin-3 on [n2+n3]-293 cells preferentially trans-interacted with nectin-2 or -3 on [n2+n3]-293 cells in the confluent state. Although the mechanism that regulates the localization of nectin-3 in the aforementioned mixed cultures remains to be elucidated, these observations corresponded with the distribution of nectin-3 in the OE from P1 onward.

Synergistic effects of combinatorial expression of nectins and cadherins on mosaic cellular patterning

We finally asked what patterns are generated by combinatorial expressing cadherins and nectins using model cell systems. To test this, we prepared 293 cells stably expressing nectin-2 and EGFP (n2-293) as a model for OCs, and 293 cells expressing nectin-3 and E-cadherin-mCherry ([n3+Ecad]-293) as a model for SCs. As mentioned in the previous section, 293 cells express N-cadherin. When n2- and n3-293 cells were examined in the mosaic-forming assay, these cells were equally intermingled with each other, resulting in a symmetrical invasion into the counter colony (Fig. 8, B and C; and Videos 3 and 4). However, in the n2- and [n3+Ecad]-293 cells, the intermingling of these cells had directionality. That is, n2-293 cells, which invaded the counter colony, lost their homotypic adhesion and were enclosed by [n3+Ecad]-293 cells. Meanwhile, [n3+Ecad]-293

Downloaded from http://rupress.org/jcb/article-pdf/212/5/561/1601018/jcb_201509020.pdf by guest on 08 February 2026

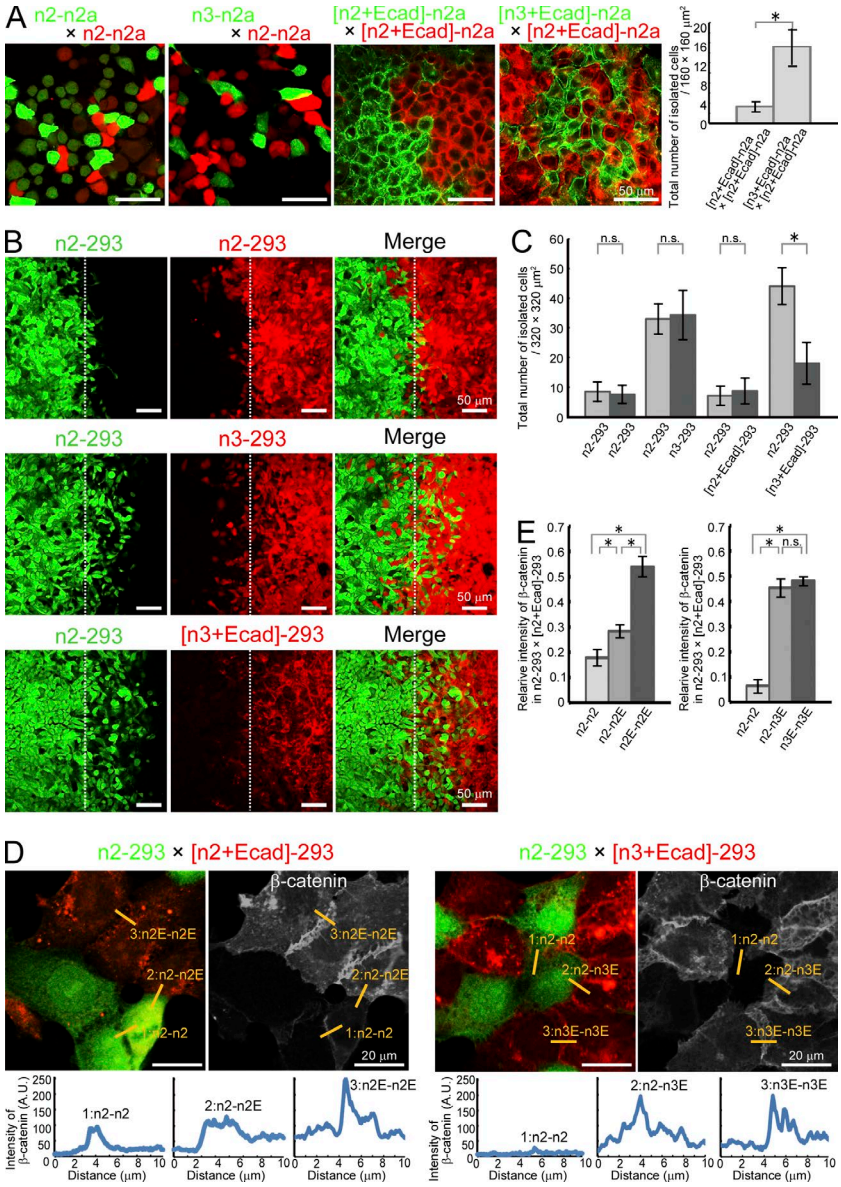

Figure 8. **Synergistic effects of combinatorial expression of nectins and cadherins on asymmetric mosaic cellular patterning.** (A) The mosaic-forming assay using neuro-2a (n2a) cells expressing different combinations of cadherins and nectins. Boundaries between the combinations of n2- and n2-n2a cells (left), n2- and n3-n2a cells (left middle), [n2+Ecad]- and [n2+Ecad]-n2a cells (right middle), and [n2+Ecad]- and [n3+Ecad]-n2a cells (right) are indicated. n2-n2a, neuro-2a nectin-2 transfectants; n3-n2a, nectin-3 transfectants; [n2+Ecad]-n2a, nectin-2 and E-cadherin transfectants; [n3+Ecad]-n2a, nectin-3 and E-cadherin transfectants. The graph shows the number of singly isolated cells in the mixtures of the two cell populations in each field. The results shown are the mean ± SD; *, $P < 0.001$; n.s., not significant. $n = 9$. (B) The mosaic-forming assay of HEK293 (293) cells expressing different cadherins and nectins. Boundaries between the combinations of n2- and n2-293 cells (top), n2- and n3-293 cells (middle), and n2- and [n3+Ecad]-293 cells (bottom) are indicated. White dotted lines indicate the center of the field. n2-293, 293 nectin-2 transfectants; n3-293, nectin-3 transfectants; [n2+Ecad]-293, nectin-2 and E-cadherin transfectants; [n3+Ecad]-293, nectin-3 and E-cadherin transfectants. (C) The graph indicates the number of singly isolated cells in the counter colony in each field. The results shown are the mean ± SD; *, $P < 0.05$. $n = 9$. (D) Distribution patterns of β-catenin in mixed cultures of n2- and [n2+Ecad]-293 (left) and n2- and [n3+Ecad]-293 cells (right). The top figures show the cellular pattern of the mixed culture (green, n2-293; red, [n2+Ecad]-293 or [n3-Ecad]-293) and immunostaining for β-catenin (white). A representative image of nine independent experiments is shown. Yellow lines indicate the positions of the densitometric tracing in the lower graphs. The graphs indicate the fluorescence intensity of β-catenin corresponding to three different homotypic or heterotypic junctions marked with the same number in the upper figures. (E) Statistical analysis for the normalized fluorescence intensity of β-catenin in mixed cultures of n2- and [n2+Ecad]-293 (left) and n2- and [n3+Ecad]-293 cells (right). Results shown are the mean ± SD; *, $P < 0.001$. $n = 9$.

cells maintained contacts with the same type of cells, whereas the population of [n3+Ecad]-293 cells detected in the counter colony was relatively small (Fig. 8, B and C; and Videos 5 and 6). In contrast, cells expressing identical nectins hardly intermingled at the border.

To understand how the directional invasion occurred, we compared the boundaries in the mixed culture of n2- and [n2+Ecad]-293 cells to that of the mixed culture of n2- and [n3+Ecad]-293 cells (Fig. 8, D and E). In the mixed culture of n2- and [n2+Ecad]-293 cells, the highest level of β-catenin was detected at homotypic junctions between [n2+Ecad]-293 cells, whereas β-catenin accumulation was low at heterotypic junctions between n2- and [n2+Ecad]-293 cells, as well as at homotypic junctions between n2-293 cells. We then examined the accumulation of β-catenin in the mixed culture of n2- and [n3+Ecad]-293 cells. β-Catenin tended to be intensely localized at heterotypic junctions between n2- and [n3+Ecad]-293 cells, as well as at homotypic junctions between [n3+Ecad]-293 cells, whereas it was faintly detected at homotypic junctions between n2-293 cells. The mosaic pattern generated by n2- and [n3+Ecad]-293 cells was reminiscent of that seen in the OE, because OCs were enclosed by SCs, whereas SCs contacted both OCs and SCs (Fig. 9 A). Thus differential adhesions between OCs and SCs were responsible for the mosaic cellular patterning of the OE.

In addition to differential adhesiveness, we suspected that differential cell mobility might also be responsible for the mosaic patterning, as our time-lapse observations revealed a significant difference in the migratory behavior of 293 cells, which was dependent of E-cadherin expression. To detect a difference in mobility between cells, we calculated their time-averaged mean square displacements. The 293 cells expressing E-cadherin migrated more slowly toward the counter colony compared with those that did not express E-cadherin (Fig. S5 A and Videos 5 and 6). The migration rates of OCs were faster than those of SCs in the mouse OE (Fig. S5 B and Video 7). These results suggested that the fast-moving cells tended to disperse toward their counterpart cells. To confirm this, we performed computer simulations of cell pattern formation (Fig. S5 C; Honda and Mochizuki, 2002). We investigated the distribution patterns of

Downloaded from http://rupress.org/jcb/article-pdf/212/5/561/1601018/jcb_201509020.pdf by guest on 08 February 2026

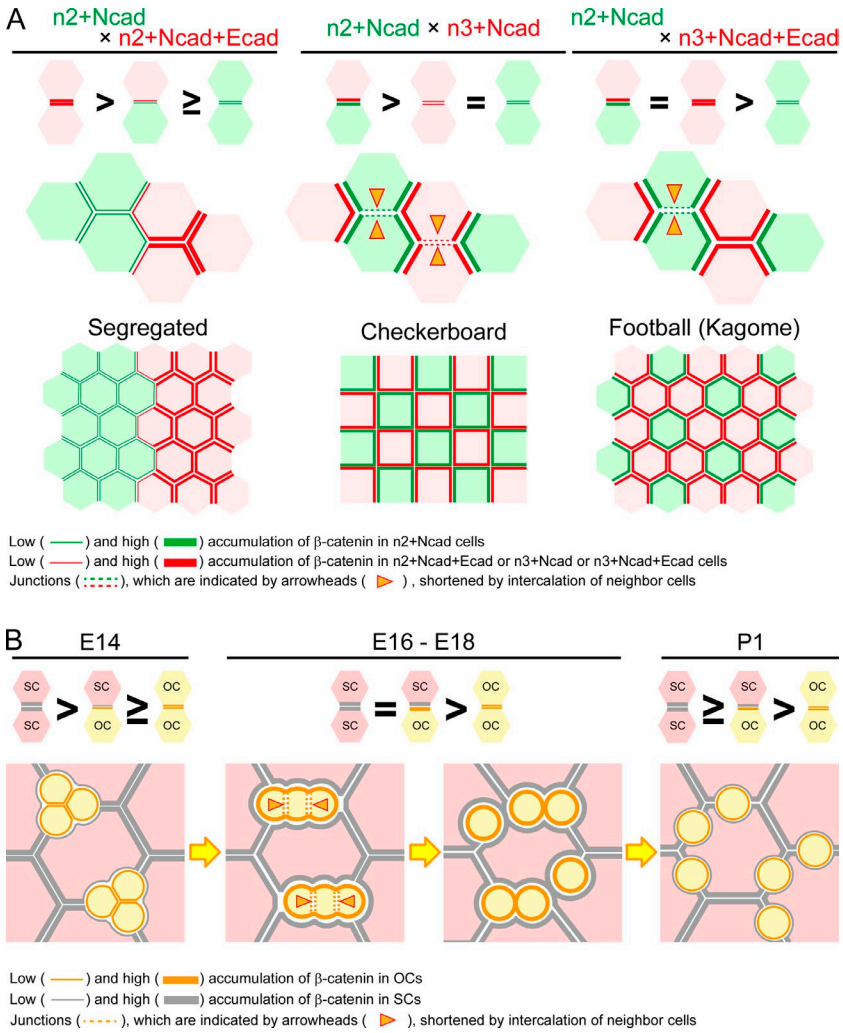

Figure 9. **Hypothetical profiles of synergistic actions of nectins and cadherins on cellular patterning.** (A) Schematic illustrations of the relative intensities of β-catenin accumulations in mixed cultures of various transfectants. Bottom panels show schematic illustrations of the cellular pattern generated by the indicated combinations of cells. See Discussion for details. (B) Schematic illustrations of the cellular patterns and the relative intensities of β-catenin accumulations in the developing OE. See Discussion for details.

two types of cells using a hexagonal lattice. In the case where heterophilic interactions were much stronger than homophilic ones, these cells intermingled bidirectionally. The measured adhesiveness of the cells, which was obtained in Fig. 8 D, was applied, which yielded the same results. We next applied the different mobility in addition to differential adhesiveness, and an asymmetric mosaic pattern was generated (Fig. 8 B). By accounting for the differential mobility, the simulations more accurately reflected actual cell behavior. These results supported the idea that differential mobility, in addition to adhesiveness, was responsible for the mosaic cellular patterning.

Discussion

In the present study, we showed that cellular rearrangements between OCs and SCs are required for mosaic cellular patterning during development. Our observations collectively suggest that the following processes govern the mosaic cellular patterning (Fig. 9 B). On E14, nectin-2 on OCs and SCs and nectin-3 on SCs homophilically trans-interact with each other. The trans-interactions of cadherins at the S-S boundary are stronger than those at the O-S and O-O boundary, resulting in the segregation of OCs and SCs. On E16, nectin-2 on OCs interacts with nectin-3 on SCs, and this trans-heterophilic interaction promotes homophilic trans-interactions of cadherins, thereby strengthening the heterotypic O-S boundary. The adhesiveness of the O-S boundary is similar to that of the S-S boundary; however, the adhesiveness of the O-O boundary is not sufficient to sustain their contacts, resulting in the separation of OCs. From E18 onward, the mosaic cellular pattern is established and maintained.

Differential expression and distribution patterns of nectins and cadherins in the OE

Our observations indicate that OCs express N-cadherin and nectin-2, whereas SCs express N-cadherin, E-cadherin, nectin-2, and nectin-3. On E14, nectin-2 on OCs mainly engages in a homophilic trans-interaction, and this homophilic trans-interaction contributes to the segregation of OCs and SCs. On E16, the heterophilic interaction between nectin-2 on OCs and nectin-3 on SCs promotes homophilic trans-interactions of cadherins via α-catenin at O-S boundary. The distribution patterns of nectin-2 on E14 are different from the theoretically conceivable combinations of the trans-interactions of nectins. As the signal for nectin-2 in the S-S and O-S boundary on E14 was weak (Fig. 3 A), the expression of nectin-2 in SCs might be low at this stage. Thus, the differential expression of nectin-2 between OCs and SCs might affect their distributions from E14 to E16. It is also known that nectins physically associate with not only afadin but also Par-3 through their PDZ binding motif (Takekuni et al., 2003), suggesting that these molecules might also contribute to cellular patterning.

Downloaded from http://rupress.org/jcb/article-pdf/212/5/561/1601018/jcb_201509020.pdf by guest on 08 February 2026

The distribution patterns of E- and N-cadherin in the OE are consistent with the molecular properties of cadherins. E- and N-cadherin are concentrated at cell–cell interfaces via homophilic trans-interactions. During development, β-catenin changes the adhesiveness of the O-S boundary. In contrast, the adhesiveness of the S-S boundary is always high. Our observations indicate that the distribution patterns of E-cadherin are stable during development; however, those of N-cadherin are dynamically changed (Figs. S2 and S3). These observations suggest that the change in adhesiveness of the O-S boundary during development is a result of the changes in N-cadherin distribution.

In αN-catenin KO mice, the number of attached OCs on P1 is larger than that in nectin KO mice. We showed that ∼20% of OCs in WT still attached to other OCs on P1 (Fig. S1 C), and this might enhance the phenotype of αN-catenin KO. However, it is possible that other cell adhesion molecules play a role in the cellular patterning in OE.

Synergistic action of nectins and cadherins in cellular patterning

In the mature OE, OCs contact SCs, whereas SCs contact OCs and SCs. These cellular patterns are reminiscent of those seen in our in vitro analysis, strongly suggesting that these cells use a similar strategy for their rearrangement. In the mixed culture of n2- and [n3+Ecad]-293 cells (Fig. 9 A, right), N-cadherin is recruited to the heterotypic boundary by the heterophilic trans-interactions between nectin-2 and -3, which are used to promote cellular intercalation. However, E-cadherin on the [n3+Ecad]-293 cells is not able to interact with n2-293 cells because n2-293 cells do not express E-cadherin. Instead, E-cadherin became concentrated at the homotypic boundary between [n3+Ecad]-293 cells. Thus, β-catenin is prominent at n2–[n3+Ecad] and [n3+Ecad]–[n3+Ecad] boundary, whereas it is reduced at the n2–n2 boundary, and this differential adhesion results in the formation of a football (also called kagome) pattern (Fig. 9 A, right).

We have previously reported that a checkerboard pattern in mouse auditory epithelium is established by the heterophilic trans-interactions between nectin-1 on hair cells and nectin-3 on supporting cells (Togashi et al., 2011). In the auditory epithelium, the expression patterns of E- and N-cadherin do not overlap, and hair cells and supporting cells express the same type of cadherin (Whitlon, 1993; Simonneau et al., 2003). In the mixed culture of n2- or n1-, and n3-293 cells, heterotypic junctions prevail and the homotypic boundary is shortened, resulting in the formation of a checkerboard pattern (Fig. 9 A, middle). Our findings suggest that combinational expression patterns of nectins and cadherins contribute to the production of complex cell patterns of sensory organs, which cannot be achieved by a single mechanism.

Differential distributions of cadherins between junctions drive cellular patterning

Our in vivo, time-lapse observations suggest that the separation of OCs might have resulted from intercalations of SCs into O-O boundary. It is known that anisotropic contractions of cell–cell junctions cause cell intercalation. During *Drosophila melanogaster* germband extension, junctions are remodeled through the polarized recruitment of myosin II within the plane of the epithelium (Bertet et al., 2004; Lecuit, 2005). The contractile activity of myosin II creates a local tension that orients the disassembly of E-cadherin junctions. In the case of neural-tube closure, a polarized constriction of neuroepithelial AJs induces the convergence of their apical domains toward the midline of the neural plate (Nishimura et al., 2012). These observations strongly suggest that anisotropic extensions and contractions of cell–cell junctions are broadly used for cellular rearrangements in the epithelial cell sheet. In the present study, we have shown that nectin-dependent differential distributions of cadherin lead to an extension or shrinkage of cell–cell junctions, thereby contributing to the cell intercalations and mosaic patterning. α-Catenin–dependent strong adhesion might provide the necessary force for SCs to intercalate between OCs. However, cooperative mechanisms between the nectin-dependent differential adhesion and the cellular mechanics (for example, actin–myosin contractility) may also play a role in mosaic cellular patterning.

Materials and methods

Mice

C57BL/6 mice were purchased from CLEA Japan. Nectin-1 KO and nectin-3 KO mice were generated by homologous recombination using targeting vectors designed to delete the exon 2 of the nectin-1 gene and the exon 1 of the nectin-3 gene, respectively (Inagaki et al., 2005). Nectin-2 KO mice were generated by homologous recombination using targeting vectors designed to replace most of exons 2 and 3 with an in-frame fusion of the LacZ gene and a selectable pgk-neo cassette (Ozaki-Kuroda et al., 2002). αN-Catenin KO mice were generated by homologous recombination using targeting vectors designed to insert IRES-EGFPpA and PGKNeopA cassettes into exon 2 of the αN-catenin gene (Togashi et al., 2002). R26-ZO1-EGFP mice (accession no. CDB0260K; http://www2.clst.riken.jp/arg/reporter_mice.html) were established from R26R-ZO1-EGFP conditional mice (accession no. CDB0225K) harboring a loxP-flanked STOP cassette in front of ZO-1-EGFP sequence (Matsuda et al., 2004) into *ROSA26* genomic locus to express under the ubiquitous transcriptional machinery (Abe et al., 2011). All the experimental procedures were approved and performed according to Kobe University Animal Experimentation Regulations (permission numbers P140108 and P121106-R1).

Tissue sample preparation

To prepare whole-mount samples of the OE from embryos and P1 mice, the OE was dissected out and fixed with 4% PFA in HBSS containing 1 mM Ca^{2+} and Mg^{2+} at 4°C for 1 h or overnight. To prepare whole-mount samples or frozen sections of the OE from mice on P28, mice were deeply anesthetized and perfused through the left ventricle with a fixative containing 4% PFA in HBSS for 20 min. Continuously, the fixative was instilled into the nostrils. The olfactory mucosa were dissected out and fixed at 4°C for 1 h. They were decapitated and post-fixed for 3 h at 4°C in the fixative and decalcified in EDTA for 5–7 d. The samples for frozen sections were cryoprotected by immersion in 30% sucrose in HBSS at 4°C and embedded in TissueTek OCT compound (Sakura Finetek) and then sectioned with a cryostat. To avoid variations in developmental growth rates between the regions of interest, the observation of the OE was restricted to the posterior ventral part of the nasal septum.

Organ culture and time-lapse imaging

Organ cultures of the OE were prepared from R26-ZO1-EGFP mouse embryos using previously described methods (Okamoto et al., 2013) with some modifications. The OE was dissected out in ice-cold DMEM and mounted in plastic dishes with collagen gel, and cultured in DMEM/F12 with 5% FBS and 5% horse serum. Time-lapse confocal microscopy was performed using a confocal scanner unit (CSU-X1; Yokogawa) equipped with an iXon+ CCD (Andor), LUMPlanFi 100×

Downloaded from http://rupress.org/jcb/article-pdf/212/5/561/1601018/jcb_201509020.pdf by guest on 08 February 2026

objective lens and an upright microscope (BX61WI; Olympus). On-stage cultures were conducted in a 40% O_2 and 5% CO_2 atmosphere at 37°C.

Immunohistochemistry

The dissected whole-mount samples after fixation and the frozen sections of the OE were permeabilized and blocked with a blocking solution containing 0.25% Triton X-100 and 5% normal goat serum in HBSS at RT for 1 h. They were incubated with primary antibodies in "Can Get Signal" immunoreaction enhancer solution (TOYOBO) at RT for 2 h. The primary antibodies were detected by fluorochrome-conjugated secondary antibodies in Can Get Signal solution at RT for 1 h. The cultured cells were fixed with 4% PFA in HBSS at 37°C for 10 min, permeabilized with 0.25% Triton X-100 in Tris-buffered saline, and blocked with 5% skim milk for 10 min. They were incubated with primary antibodies in 5% skim milk for 90 min. The primary antibodies were detected by fluorochrome-conjugated secondary antibodies in 5% skim milk for 45 min. The following primary antibodies were used: anti–ZO-1 rat mAb (clone R40.76, 1:200 dilution; Merck Millipore), anti–E-cadherin rat mAb (clone ECCD2, 1:1,000 dilution; a gift from M. Takeichi, RIKEN Center for Developmental Biology, Kobe, Japan), anti–E-cadherin mouse mAb (1:200 dilution; BD Transduction Laboratories), anti-N-cadherin mouse mAb (1:100 dilution; BD Transduction Laboratories), anti-β-catenin mouse mAb (1:200 dilution; clone 5H10, Merck Millipore), anti–αN-catenin rat mAb (clone NCAT2, 1:200 dilution; a gift from M. Takeichi), anti–αE-catenin rat mAb (clone α18, 1:50 dilution; a gift from A. Nagafuchi), anti–nectin-1 rat mAb (clone 48–12; MBL), anti–nectin-2 rat mAb (clone 502–57; MBL), anti–nectin-3 rat mAb (clone 103-A1; MBL), and anti–l-afadin rabbit antibody (Sigma-Aldrich). Primary antibodies were visualized with Alexa Fluor 488–, Alexa Fluor 647– (Invitrogen), and Cy3-conjugated (Merck Millipore) secondary goat antibodies. Samples were mounted in glycerol gelatin (Sigma-Aldrich) or FluorSave Reagent (Merck Millipore). Images were obtained with a confocal microscope (LSM700; Carl Zeiss) equipped with a 40× NA 1.2 or a 40× NA 1.3 lens using ZEN software (Carl Zeiss), and these images were analyzed with the same software and processed with Adobe Photoshop.

In situ hybridization

To prepare paraffin embedded sections of the OE of P28 mice, P28 mice were fix by vascular perfusion with 4% PFA in HBSS, then decapitated and fixed with 4% PFA in HBSS at RT for 72 h. The tissues were embedded into paraffin and cut into 5-µm-thick tissue sections using a rotary microtome. In situ hybridization was performed using the Quanti Gene View RNA kit (Panomics) according to the manufacturer's recommendations. The RNA targets were mouse genes pvrl1, pvrl2, pvrl3, cdh1, and cdh2. The signals for the expression of these RNAs were detected using Fast RED. Nuclei were counterstained with DAPI, and OCs were immunostained with anti-OMP goat antibody (WAKO).

Quantification of junctional intensity

Measurements of intensity of cell–cell junctions in the mouse OE were performed by quantifying the pictures of specimens using Metamorph software (Molecular Devices). In Fig. S2, quantifications were performed for normalized fluorescence intensities, and the mean and SDs were calculated. In Figs. 5 E and 8 E, quantifications were performed for normalized fluorescence intensities, and the mean was calculated. Then, F test was performed to quantify the magnitude of the changes, and the Student's or Welch's *t* test was performed to determine if there was a significant change.

Expression vectors

cDNAs for mouse nectins and cadherins were used throughout the experiments. To construct the expression vector, we subcloned each cDNA fragment into pCANw, pCAH, and pCAB vectors (Ichii and Takeichi, 2007). These expression vectors were used for stable expression in eukaryotic cells, in which a neomycin, hygromycin, or blasticidin resistance gene was driven by the internal ribosomal entry site element. The generation of nectin-ΔPDZ constructs was described previously (Takahashi et al., 1999). The generation of E- or N-cadherin fused with EGFP or mCherry constructs was subcloned cDNAs of cadherins into pCANw-EGFP or pCANw-mCherry (Ichii and Takeichi, 2007).

Mosaic forming assay and time-lapse microscopy of cultured cells

Cultures were maintained in DMEM/F-12 with 10% fetal calf serum. In the mosaic-forming assays, culture inserts (Ibidi) were used. Each insert was filled with several cells transfected with EGFP or mCherry. The cells were fixed for 72–96 h after inserts were removed. The number of isolated single cells appearing in the adjacent territory was counted for each combination, and the results were statistically analyzed by Welch's *t* test. In the coculture experiments, the two types of cells were dissociated into single cells, mixed at a ratio of 1:1, and cultured for the cells to grow into adequate large colonies. In Fig. 8 B, the number of isolated single cells appearing in the colonies of the other cells was counted for each combination, and the results were statistically analyzed by Welch's *t* test. Time-lapse imaging was performed using the LCV110 incubator microscope system equipped with an EMCCD camera (ImagEM; Hamamatsu) in a combination with a spinning disc laser scan system (CSU-X1; Yokogawa) and Metamorph software. Before experiments, the cells were seeded onto thin-bottom plastic dishes (Ibidi) and observed with a 20 × 0.75 NA lens.

Computer simulation of mosaic cellular patterning

The vertex dynamics for polygonal cells were used for computer simulation, and they had differential equations to calculate coordinates of vertices of polyhedra (Honda et al., 2008). The differential equations were modified for calculation of coordinates of vertices of polygons on surface of a sheet in 3D space. The differential equations contain a potential U and the vertices migrate so that the potential U becomes small; that is, the system becomes stable. The potential U involves an elastic term of areas of the polygons and adhesiveness terms of cell boundaries. The elastic term is $\rho \Sigma_i (S_i - S_o)^2$, where ρ is the relative coefficient of polygon deformation, Si is an area of polygon i, and So is a standard or relaxed polygon area. The adhesiveness terms are $1/a_{oo} L_{oo} + 1/a_{os} \Sigma_{jos} L_{jos} + 1/a_{ss} \Sigma_{jss} L_{jss}$, where a_{oo}, a_{so}, and a_{ss} are adhesiveness strengths of polygon edges O-O, O-S, and S-S; L_{oo} is length of edge O-O; j_{os} and j_{ss} are identification numbers of edges O-S and S-S, respectively; and L_{jos} and L_{jss} are lengths of edges j_{os} and j_{ss}, respectively. The computer simulation of Fig. 4 B was performed under the condition that the relative coefficient of polygon deformation is $\rho = 10.0$ and the adhesiveness strengths are $a_{oo} = 0.533$ and $a_{ss} = 1.0$. The adhesiveness strengths of boundary O-S, a_{os}, were 1.0 (Fig. 6 B, left, 0–2,300 steps), 0.89 (Fig. 6 B, left, 2,300–4,000 steps), and 0.833 (Fig. 6 B, right).

Quantification of cell mobility

To show the difference in mobility of the cells, we calculated the time-averaged mean square displacements using Metamorph and Microsoft Excel (Fig. S5, A and B). Note that this quantity is a simple mean over time so that the value may differ from ordinary MSD used in the context of diffusive processes. We first collected the square displacements of OCs, or SCs, from different time windows for a given time lapse and then averaged them over time. Then, the Student's *t* test was performed to determine if there was a significant change. This procedure was considered to be sufficient for manifesting the mobility difference between OC and SC, although stage-dependent details of the cellular movements were to be smeared out by this averaging procedure.

Downloaded from http://rupress.org/jcb/article-pdf/212/5/561/1601018/jcb_201509020.pdf by guest on 08 February 2026

Investigation of asymmetric distribution of two types of cells using a hexagonal lattice

We investigated distribution patterns of two types of cells using a hexagonal lattice (32 × 32 cells) where green hexagons (G) and red hexagons (R) were situated in the left and right half sides, respectively. A hexagon had six boundaries, and each boundary had its own adhesiveness strength (a_{GG}, a_{GR}, and a_{RR}), depending on species of the hexagon and species of neighboring hexagons (G or R). When cells performed local rearrangement, the adhesiveness strength of boundary changed. We assumed that cell rearrangements took place so that the total adhesiveness strength increased. After repetition of the local cell rearrangements at random, we obtained more stable cell patterns (Honda and Mochizuki, 2002). We investigated what condition produced the asymmetric distribution pattern, as shown in Fig. 8 B.

Detailed procedure of the local cell rearrangements is described below. At first, we defined an aggregate of four hexagons at random as follows. After picking up hexagon A at random in the hexagonal lattice, we made six aggregates of four hexagons that involved hexagon A (Fig. S5 D). Then, we chose an aggregate among the six aggregates at random. We defined an aggregate. Next, we calculated the total adhesiveness strength of four hexagons in the aggregate (a_{ini}). By permutation of four hexagons within the aggregate, we got 24 ways of four-hexagon arrangements (4! = 24). We calculated the total adhesiveness strength of four hexagons in each aggregate and obtained an aggregate having the maximum adhesiveness strength (a_{max}). Increase of the adhesive strength during the local rearrangement of hexagons was $\Delta = a_{max} - a_{ini}$. The local cell rearrangement actually took place using the probability. The probability was determined by the formula, $1/[1+\exp(-\Delta)]$, that is, when the cell adhesiveness strength largely increased, such local cell rearrangement took place with high probability. We obtained a cell pattern after repetitions of 10,000 or 12,000 steps. The cell pattern was under construction to a final pattern.

There were two ways to pick up hexagon A at the beginning of each local cell rearrangement. When we assumed that hexagon G and hexagon R behaved in the same mobility, we picked up hexagon A among hexagons G and R at random. When we assumed that hexagon G behaved differently in the mobility, e.g., faster than hexagon R, we picked up hexagon A among hexagon Gs. Hexagon R behaved passively through the behavior of hexagon G.

We show the results of computer simulations producing asymmetric distribution of two types of cells in the hexagonal lattice. We examined whether differential adhesiveness and cell mobility were implicated in asymmetric mosaic pattern formation. Hexagons G and R were placed on the left and right half domains on the hexagonal lattice. We first performed a simulation in the case where the same adhesiveness intensity worked between all hexagons ($\{a_{GG}, a_{GR}, a_{RR}\}$. = {1.0, 1.0, 1.0}). A hexagon was chosen among the hexagons G and R at random, assuming that hexagons G and R behaved in the same mobility as described previously. After many repetitions of the hexagon rearrangement, we obtained mosaic cell patterns (Fig. S5 C, left). The hexagons fluctuated at random a little, but there was no tendency for one type of hexagon to enclose another type of hexagon (compared with the following three patterns). We defined the asymmetry index to know the degree of asymmetric distribution (left and right sides) of two types of hexagons as mentioned later. Asymmetry index was 1.00; that is, it indicated complete symmetry.

Then, we introduced differential adhesiveness between the hexagons and obtained results (Fig. S5 C, left middle). In the case where heterophilic interactions (a_{GR}) were much stronger than homophilic ones (a_{GG}, a_{RR}), $\{a_{GG}, a_{GR}, a_{RR}\}$ = {0.5, 1.0, 0.5} and a hexagon was chosen among the hexagons G and R at random, hexagons actively intermingled bidirectionally (to left and right sides). Asymmetry index was 0.93; that is, almost symmetry. There was clear tendency for one type of hexagons to enclose another type of hexagons. Then, the measured adhesiveness value of the cells, which was calculated for the HEK293 cells in Fig. 8 C, were applied ($\{a_{GG}, a_{GR}, a_{RR}\}$ = {0.1, 1.0, 1.0} and a hexagon was chosen at random). The results showed that these cells also actively intermingled bidirectionally (Fig. S5 C, right middle). The pattern was symmetrical (asymmetry index was 0.94). There was also clear tendency to enclose another type of hexagons. We then applied the differential mobility between the cells (Fig. S5, A and B), in addition to the differential adhesiveness. To reflect the difference in the mobility of the cells, we modified the random step choice of the cells by preferentially choosing hexagon G. We examined the cellular pattern using the modified procedure and found that an asymmetric mosaic pattern was generated (Fig. S5 C, right). The asymmetry index was 1.46, indicating that the infiltration distance of hexagon G was greater than that of hexagon R when hexagon G was preferentially chosen. These results supported the idea that differential mobility was also responsible for asymmetric mosaic cellular patterning. Collectively, both the differential adhesiveness and mobility of the cells in the OE cooperatively regulated the cellular rearrangement of the OE.

Definition of the asymmetry index

To show the degree of asymmetry of cell distribution quantitatively, we defined the index of asymmetry as follows. Coordinates of the left and right sides of the area were x = 0 and 100, respectively. The area was divided into left and right domains. Some of hexagons migrated from the left domain to the right domain. Their number was n_L and their gravity center along the x axis was g_L. Number of cells that migrated from the right domain to the left domain was n_R, and their gravity center along the x axis was g_R. The gravity centers were defined by $g_L = 1/n_L \Sigma_i n_L x_i$ and $g_R = 1/n_R \Sigma_i n_R x_i$. The asymmetry index was $(g_R - 50)/(50 - g_L)$. When the asymmetry index was larger than 1, equal to 1, or smaller than 1, the cell distribution was right asymmetry, symmetry, or left asymmetry, respectively.

Online supplemental material

Fig. S1 shows the schematic illustration of mouse OE. Fig. S2 shows the summary of distribution patterns of nectins, cadherins, and catenins in the developing mouse OE. Fig. S3 shows the distribution change of cadherins in the developing mouse OE. Fig. S4 shows nectin and β-catenin distribution in a mixed culture of nectin transfectants. Fig. S5 shows asymmetric distribution of two types of cells using a hexagonal lattice. Video 1 shows time-lapse microscopy of the organ culture of the OE prepared at E14 from R26-ZO1-EGFP mice. Video 2 shows time-lapse microscopy of a coculture of neuro-2a cells expressing E-cadherin and EGFP and those expressing N-cadherin and mCherry. Video 3 shows time-lapse microscopy of a mosaic-forming assay of HEK293 cells expressing nectin-3 and EGFP and those expressing nectin-3 and mCherry. Video 4 shows time-lapse microscopy of a mosaic-forming assay of HEK293 cells expressing nectin-1 and EGFP and those expressing nectin-3 and mCherry. Video 5 shows time-lapse microscopy of a mosaic-forming assay of HEK293 cells expressing nectin-3 and mCherry and those expressing nectin-3 and E-cadherin-EGFP. Video 6 shows time-lapse microscopy of a mosaic-forming assay of HEK293 cells expressing nectin-1 and mCherry and those expressing nectin-3 and E-cadherin-EGFP. Video 7 shows time-lapse microscopy of the organ culture of the OE prepared at E14 from R26-ZO1-EGFP mice. Online supplemental material is available at http://www.jcb.org/cgi/content/full/jcb.201509020/DC1.

Downloaded from http://rupress.org/jcb/article-pdf/212/5/561/1601018/jcb_201509020.pdf by guest on 08 February 2026

Acknowledgments

We are grateful to T. Miura, K. Sato, T. Shibata, and M. Takeichi for discussions; T. Fujimori and S. Tsukita for support in generating the R26-ZO1-EGFP mice; and Y. Kurihara, S. Hiver, and H. Saito for their technical support. We thank the RIKEN Integrated Cluster of Clusters and the Institute of Statistical Mathematics for their supercomputation facilities.

This work was supported by Japan Society for the Promotion of Science KAKENHI grants 15K10782, 21227005, 21570234, 22111001, 22791599, 24390388, 24791777, 25111716, 25127710, 25440117, 25440107, and 26540158; by the Global COE Program "Global Center for Education and Research in Integrative Membrane Biology;" by the Targeted Proteins Research Program; and by a grant from the Takeda Science Foundation.

The authors declare no competing financial interests.

Submitted: 3 September 2015
Accepted: 21 January 2016

References

Abe, T., H. Kiyonari, G. Shioi, K. Inoue, K. Nakao, S. Aizawa, and T. Fujimori. 2011. Establishment of conditional reporter mouse lines at ROSA26 locus for live cell imaging. *Genesis.* 49:579–590. http://dx.doi.org/10.1002/dvg.20753

Bertet, C., L. Sulak, and T. Lecuit. 2004. Myosin-dependent junction remodelling controls planar cell intercalation and axis elongation. *Nature.* 429:667–671. http://dx.doi.org/10.1038/nature02590

Cuschieri, A., and L.H. Bannister. 1975. The development of the olfactory mucosa in the mouse: electron microscopy. *J. Anat.* 119:471–498.

Fabre, S., N. Reymond, F. Cocchi, L. Menotti, P. Dubreuil, G. Campadelli-Fiume, and M. Lopez. 2002. Prominent role of the Ig-like V domain in trans-interactions of nectins. Nectin3 and nectin 4 bind to the predicted C-C'-C"-D beta-strands of the nectin1 V domain. *J. Biol. Chem.* 277:27006–27013. http://dx.doi.org/10.1074/jbc.M203228200

Foty, R.A., and M.S. Steinberg. 2005. The differential adhesion hypothesis: a direct evaluation. *Dev. Biol.* 278:255–263. http://dx.doi.org/10.1016/j.ydbio.2004.11.012

Harrison, O.J., J. Vendome, J. Brasch, X. Jin, S. Hong, P.S. Katsamba, G. Ahlsen, R.B. Troyanovsky, S.M. Troyanovsky, B. Honig, and L. Shapiro. 2012. Nectin ectodomain structures reveal a canonical adhesive interface. *Nat. Struct. Mol. Biol.* 19:906–915. http://dx.doi.org/10.1038/nsmb.2366

Hirano, S., N. Kimoto, Y. Shimoyama, S. Hirohashi, and M. Takeichi. 1992. Identification of a neural alpha-catenin as a key regulator of cadherin function and multicellular organization. *Cell.* 70:293–301. http://dx.doi.org/10.1016/0092-8674(92)90103-J

Hogan, C., N. Serpente, P. Cogram, C.R. Hosking, C.U. Bialucha, S.M. Feller, V.M. Braga, W. Birchmeier, and Y. Fujita. 2004. Rap1 regulates the formation of E-cadherin-based cell-cell contacts. *Mol. Cell. Biol.* 24:6690–6700. http://dx.doi.org/10.1128/MCB.24.15.6690-6700.2004

Honda, H., and A. Mochizuki. 2002. Formation and maintenance of distinctive cell patterns by coexpression of membrane-bound ligands and their receptors. *Dev. Dyn.* 223:180–192. http://dx.doi.org/10.1002/dvdy.10042

Honda, H., M. Tanemura, and T. Nagai. 2004. A three-dimensional vertex dynamics cell model of space-filling polyhedra simulating cell behavior in a cell aggregate. *J. Theor. Biol.* 226:439–453. http://dx.doi.org/10.1016/j.jtbi.2003.10.001

Honda, H., T. Nagai, and M. Tanemura. 2008. Two different mechanisms of planar cell intercalation leading to tissue elongation. *Dev. Dyn.* 237:1826–1836. http://dx.doi.org/10.1002/dvdy.21609

Ichii, T., and M. Takeichi. 2007. p120-catenin regulates microtubule dynamics and cell migration in a cadherin-independent manner. *Genes Cells.* 12:827–839. http://dx.doi.org/10.1111/j.1365-2443.2007.01095.x

Inagaki, M., K. Irie, H. Ishizaki, M. Tanaka-Okamoto, K. Morimoto, E. Inoue, T. Ohtsuka, J. Miyoshi, and Y. Takai. 2005. Roles of cell-adhesion molecules nectin 1 and nectin 3 in ciliary body development. *Development.* 132:1525–1537. http://dx.doi.org/10.1242/dev.01697

Katsamba, P., K. Carroll, G. Ahlsen, F. Bahna, J. Vendome, S. Posy, M. Rajebhosale, S. Price, T.M. Jessell, A. Ben-Shaul, et al. 2009. Linking molecular affinity and cellular specificity in cadherin-mediated adhesion. *Proc. Natl. Acad. Sci. USA.* 106:11594–11599. http://dx.doi.org/10.1073/pnas.0905349106

Lecuit, T. 2005. Adhesion remodeling underlying tissue morphogenesis. *Trends Cell Biol.* 15:34–42. http://dx.doi.org/10.1016/j.tcb.2004.11.007

Martinez-Rico, C., F. Pincet, E. Perez, J.P. Thiery, K. Shimizu, Y. Takai, and S. Dufour. 2005. Separation force measurements reveal different types of modulation of E-cadherin-based adhesion by nectin-1 and -3. *J. Biol. Chem.* 280:4753–4760. http://dx.doi.org/10.1074/jbc.M412544200

Matsuda, M., A. Kubo, M. Furuse, and S. Tsukita. 2004. A peculiar internalization of claudins, tight junction-specific adhesion molecules, during the intercellular movement of epithelial cells. *J. Cell Sci.* 117:1247–1257. http://dx.doi.org/10.1242/jcs.00972

Nishimura, T., H. Honda, and M. Takeichi. 2012. Planar cell polarity links axes of spatial dynamics in neural-tube closure. *Cell.* 149:1084–1097. http://dx.doi.org/10.1016/j.cell.2012.04.021

Nose, A., A. Nagafuchi, and M. Takeichi. 1988. Expressed recombinant cadherins mediate cell sorting in model systems. *Cell.* 54:993–1001. http://dx.doi.org/10.1016/0092-8674(88)90114-6

Okamoto, M., T. Namba, T. Shinoda, T. Kondo, T. Watanabe, Y. Inoue, K. Takeuchi, Y. Enomoto, K. Ota, K. Oda, et al. 2013. TAG-1-assisted progenitor elongation streamlines nuclear migration to optimize subapical crowding. *Nat. Neurosci.* 16:1556–1566. http://dx.doi.org/10.1038/nn.3525

Ozaki-Kuroda, K., H. Nakanishi, H. Ohta, H. Tanaka, H. Kurihara, S. Mueller, K. Irie, W. Ikeda, T. Sakai, E. Wimmer, et al. 2002. Nectin couples cell-cell adhesion and the actin scaffold at heterotypic testicular junctions. *Curr. Biol.* 12:1145–1150. http://dx.doi.org/10.1016/S0960-9822(02)00922-3

Sato, T., N. Fujita, A. Yamada, T. Ooshio, R. Okamoto, K. Irie, and Y. Takai. 2006. Regulation of the assembly and adhesion activity of E-cadherin by nectin and afadin for the formation of adherens junctions in Madin-Darby canine kidney cells. *J. Biol. Chem.* 281:5288–5299. http://dx.doi.org/10.1074/jbc.M510070200

Satoh-Horikawa, K., H. Nakanishi, K. Takahashi, M. Miyahara, M. Nishimura, K. Tachibana, A. Mizoguchi, and Y. Takai. 2000. Nectin-3, a new member of immunoglobulin-like cell adhesion molecules that shows homophilic and heterophilic cell-cell adhesion activities. *J. Biol. Chem.* 275:10291–10299. http://dx.doi.org/10.1074/jbc.275.14.10291

Simonneau, L., M. Gallego, and R. Pujol. 2003. Comparative expression patterns of T-, N-, E-cadherins, beta-catenin, and polysialic acid neural cell adhesion molecule in rat cochlea during development: implications for the nature of Kölliker's organ. *J. Comp. Neurol.* 459:113–126. http://dx.doi.org/10.1002/cne.10604

Steinberg, M.S. 2007. Differential adhesion in morphogenesis: a modern view. *Curr. Opin. Genet. Dev.* 17:281–286. http://dx.doi.org/10.1016/j.gde.2007.05.002

Steinke, A., S. Meier-Stiegen, D. Drenckhahn, and E. Asan. 2008. Molecular composition of tight and adherens junctions in the rat olfactory epithelium and fila. *Histochem. Cell Biol.* 130:339–361. http://dx.doi.org/10.1007/s00418-008-0441-8

Tachibana, K., H. Nakanishi, K. Mandai, K. Ozaki, W. Ikeda, Y. Yamamoto, A. Nagafuchi, S. Tsukita, and Y. Takai. 2000. Two cell adhesion molecules, nectin and cadherin, interact through their cytoplasmic domain-associated proteins. *J. Cell Biol.* 150:1161–1176. http://dx.doi.org/10.1083/jcb.150.5.1161

Takahashi, K., H. Nakanishi, M. Miyahara, K. Mandai, K. Satoh, A. Satoh, H. Nishioka, J. Aoki, A. Nomoto, A. Mizoguchi, and Y. Takai. 1999. Nectin/PRR: an immunoglobulin-like cell adhesion molecule recruited to cadherin-based adherens junctions through interaction with Afadin, a PDZ domain-containing protein. *J. Cell Biol.* 145:539–549. http://dx.doi.org/10.1083/jcb.145.3.539

Takai, Y., and H. Nakanishi. 2003. Nectin and afadin: novel organizers of intercellular junctions. *J. Cell Sci.* 116:17–27. http://dx.doi.org/10.1242/jcs.00167

Takai, Y., W. Ikeda, H. Ogita, and Y. Rikitake. 2008. The immunoglobulin-like cell adhesion molecule nectin and its associated protein afadin. *Annu. Rev. Cell Dev. Biol.* 24:309–342. http://dx.doi.org/10.1146/annurev.cellbio.24.110707.175339

Takeichi, M. 1990. Cadherins: a molecular family important in selective cell-cell adhesion. *Annu. Rev. Biochem.* 59:237–252. http://dx.doi.org/10.1146/annurev.bi.59.070190.001321

Takeichi, M. 2011. Self-organization of animal tissues: cadherin-mediated processes. *Dev. Cell.* 21:24–26. http://dx.doi.org/10.1016/j.devcel.2011.06.002

Takekuni, K., W. Ikeda, T. Fujito, K. Morimoto, M. Takeuchi, M. Monden, and Y. Takai. 2003. Direct binding of cell polarity protein PAR-3 to cell-

Downloaded from http://rupress.org/jcb/article-pdf/212/5/561/1601018/jcb_201509020.pdf by guest on 08 February 2026

cell adhesion molecule nectin at neuroepithelial cells of developing mouse. *J. Biol. Chem.* 278:5497–5500. http://dx.doi.org/10.1074/jbc.C200707200

Togashi, H., K. Abe, A. Mizoguchi, K. Takaoka, O. Chisaka, and M. Takeichi. 2002. Cadherin regulates dendritic spine morphogenesis. *Neuron.* 35:77–89. http://dx.doi.org/10.1016/S0896-6273(02)00748-1

Togashi, H., J. Miyoshi, T. Honda, T. Sakisaka, Y. Takai, and M. Takeichi. 2006. Interneurite affinity is regulated by heterophilic nectin interactions in concert with the cadherin machinery. *J. Cell Biol.* 174:141–151. http://dx.doi.org/10.1083/jcb.200601089

Togashi, H., K. Kominami, M. Waseda, H. Komura, J. Miyoshi, M. Takeichi, and Y. Takai. 2011. Nectins establish a checkerboard-like cellular pattern in the auditory epithelium. *Science.* 333:1144–1147. http://dx.doi.org/10.1126/science.1208467

Watabe, M., A. Nagafuchi, S. Tsukita, and M. Takeichi. 1994. Induction of polarized cell-cell association and retardation of growth by activation of the E-cadherin-catenin adhesion system in a dispersed carcinoma line. *J. Cell Biol.* 127:247–256. http://dx.doi.org/10.1083/jcb.127.1.247

Whitlon, D.S. 1993. E-cadherin in the mature and developing organ of Corti of the mouse. *J. Neurocytol.* 22:1030–1038. http://dx.doi.org/10.1007/BF01235747

Yasumi, M., K. Shimizu, T. Honda, M. Takeuchi, and Y. Takai. 2003. Role of each immunoglobulin-like loop of nectin for its cell-cell adhesion activity. *Biochem. Biophys. Res. Commun.* 302:61–66. http://dx.doi.org/10.1016/S0006-291X(03)00106-2

Downloaded from http://rupress.org/jcb/article-pdf/212/5/561/1601018/jcb_201509020.pdf by guest on 08 February 2026